The Molecularly Controlled Synthesis of Ordered Bi-dimensional C60 Arrays

Gengler, Regis Y. N.; Gournis, Dimitrios; Aimon, Akfiny H.; Toma, Luminita M.; Rudolf, Petra

Published in:
Chemistry

DOI:
10.1002/chem.201103528

Publication date:
2012

CHEMISTRY
A EUROPEAN JOURNAL

ChemPubSoc
Europe

DOI: 10.1002/chem.201103528

The Molecularly Controlled Synthesis of Ordered Bi-dimensional C_{60} Arrays

Régis Y. N. Gengler,*[a] Dimitrios Gournis,[a, b] Akfiny H. Aimon,[a] Luminita M. Toma,[a] and Petra Rudolf*[a]

Abstract: Much of the research effort concerning the nanoscopic properties of clays has focused on its mechanical applications, for example, as nanofillers for polymer reinforcement. To broaden the horizon of what is possible by exploiting the richness of clays in nanoscience, herein we report a bottom-up approach for the production of hybrid materials in which clays act as the structure-directing interface and reaction media. This new method, which combines self-assembly with the Langmuir–Schaefer technique, uses the clay nanosheets as a template for the grafting of C_{60} into a bi-dimensional array, and allows for perfect layer-by-layer growth with control at the molecular level. In contrast to the more-common growth of C_{60} arrays through nanopatterning, our approach can be performed under atmospheric conditions, can be upscaled to areas of tenths of cm^2, and can be applied to almost any hydrophobic substrate. Herein, we report a detailed study of this approach by using temperature-dependent X-ray diffraction, spectroscopic measurements, and STM.

Keywords: clays · fullerenes · nanostructures · self-assembly

Introduction

In recent years, low-dimensional assemblies, in which order and organization follow supramolecular principles, have assumed remarkable importance owing to their outstanding physical and/or chemical and/or biological properties, which make them attractive candidates for applications in many fields, ranging from photophysics and electronics to catalysis, molecular separation, as well as drug delivery and biosensing.[1] Controlling both the organization of the assemblies and their physical and chemical properties through simple external parameters has led to the creation of new tailored functional materials.[2] Top-down methods that were based on photolithography were largely developed for the manufacture of integrated circuits (ICs) and were found to be practical for inorganic materials and metals but less suitable for controlling the nanostructuring of organic building blocks.

An alternative method is the bottom-up approach in which, by imitating the strategies of biological self-assembly, one can create entirely new molecular building blocks and form supramolecular architectures whose final structure is encoded in the shape and properties of the clusters or molecules that are used. In particular, molecular alignment in a 2D assembly can be tuned to modify the physical and chemical properties of the resulting material.[2,11,21–27,29] Thin films that were grown by deposition under ultrahigh vacuum are a much-exploited example of this behavior in which the initial monolayer maximizes the van der Waals and Coulomb forces to produce flat adsorption, whilst the subsequent deposition often makes molecules stand up.[3] However, islanding, which results in both 2D and 3D arrangements, is not easily avoidable with this fabrication method.

Herein, we adopt an alternative approach that is based on one of the most-common, although not widely employed, materials, namely layered smectite clay, with the aim of developing and studying highly ordered 2D assemblies of carbon-based nanostructured systems, such as fullerenes. Natural and synthetic smectite clays are composed of stacked nanometer-sized aluminosilicate platelets and present a unique combination of swelling, intercalation, and ion-exchange properties that make them valuable in diverse applications.[4,5] Each platelet consists of an octahedral alumina layer that is fused between two tetrahedral silica layers. The 1 nm thick platelets are negatively charged and a neutral overall charge is obtained, for example, by the presence of hydrated cations between adjacent platelets. The intercalation process in these systems is equivalent to ion-exchange. Unlike intercalation compounds of graphite it does not necessarily involve charge-transfer between the guest and host species. These materials have the natural ability to adsorb organic or inorganic guest cationic species (and even neutral molecules) from solution. It is this cation "storage" that

[a] Dr. R. Y. N. Gengler, Prof. Dr. D. Gournis, A. H. Aimon, Dr. L. M. Toma, Prof. Dr. P. Rudolf
Zernike Institute for Advanced Materials
University of Groningen
Nijenborg 4, NL-9747AG Groningen (The Netherlands)
Fax: (+31) 50 363 7208
E-mail: p.rudolf@rug.nl
regis.gengler@desy.de

[b] Prof. Dr. D. Gournis
Department of Materials Science and Engineering
University of Ioannina, GR-45110, Ioannina (Greece)

Supporting information for this article is available on the WWW under http://dx.doi.org/10.1002/chem.201103528.

gives clay minerals their unique properties and forms the basis of their use as catalysts,[6] templates in organic synthesis,[7,8] or as building blocks for composite materials.[9–12] The nature of the microenvironment between the aluminosilicate sheets regulates the topology of the intercalated molecules and affects any possible supramolecular rearrangements or reactions, such as self-assembly processes that are not easily controlled in the solution state.[10–12]

Fullerenes and their derivatives exhibit an extremely rich collection of interesting and potentially useful physical properties: they are excellent electron acceptors, can be transformed into synthetic metals, exhibit superconductivity[13] at transition temperatures that are only exceeded by those of cuprates, support ferromagnetism[14] (without the presence of d or f electrons), and display remarkable non-linear-optical behavior.[15] Considerable effort has been made to develop C_{60}-based assemblies and supramolecular nanostructures.[16,17] However, fullerenes spontaneously aggregate when deposited onto solid surfaces on which they are not strongly chemisorbed. In spite of this drawback, when fullerene molecules are placed between clay layers, the microenvironment of the interlayer space can inhibit aggregation of the C_{60} cages and allow the study of 2D structures of these molecules. Recently,[18,19] we described the insertion and subsequent behavior of a series of water-soluble fullerene derivatives into the interlayer space of clay wherein a relatively high density and a high degree of ordering were achieved. Fulleropyrrolidine monoadduct and bisadduct derivatives, which were positively charged and water-soluble, were introduced into the clay galleries through simple ion-exchange in the bulk phase. These experiments, which were complemented by computer simulations, revealed the successful intercalation of fulleropyrrolidine derivatives and demonstrated that these hybrid systems possessed interesting optical and electronic properties. Over the past decade, a method that combines self-assembly and the Langmuir–Blodgett assembly has emerged and enabled the layer-by-layer growth of clay hybrids.[2,20] Owing to the spatial arrangement of the clay platelets, such an assembly leads to control on the nanoscale and retains order on the macroscale. Although this emerging field of clay nanoscience remains largely unexplored, several studies have demonstrated the successful integration of a variety of guest species within the clay thin-film structure that was either synthesized on the clay surfaces through a cation-exchange-driven self-assembly process or through the integration of functional molecules.[2,11,21–29]

Herein, we report the synthesis of ordered bi-dimensional arrays of C_{60} molecules that were sandwiched between clay layers by means of a modified (hybrid) Langmuir–Schaefer method. Our film-preparation approach involves a bottom-up layer-by-layer process (Figure 1) that includes the formation of a hybrid amphiphilic-cation–clay-mineral Langmuir film, which hosts C_{60} molecules within its interlayer spacing. This assembly of the clay stack with its guest molecules is afforded through a succession of charge-driven functionalization (or self-assembly) steps that exploit the templating properties of the clay.

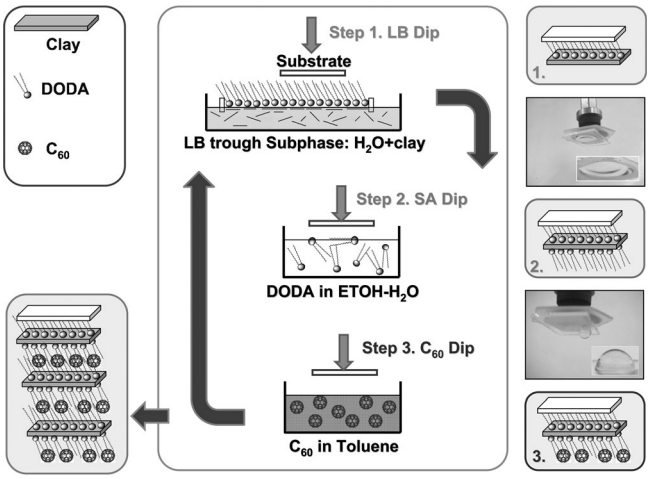

Figure 1. Top left: Explanation of the symbols for the different materials; clay = montmorillonite Kunipia F (structural formula: $Ca_{0.11}Na_{0.891}(Si_{7.63}Al_{0.37})(Al_{3.053}Mg_{0.65}Fe_{0.245}Ti_{0.015})\cdot O_{20}(OH)_4$), DODA = dimethyldioctadecylammonium (structural formula: $[\{CH_3(CH_2)_{17}\}_2N(Br)(CH_3)_2]$). Central panel: The deposition cycle for DODA–clay–DODA–C_{60} films. Step 1: Transfer of the DODA–clay monolayer onto a substrate. Step 2: Creation of a self-assembled monolayer of DODA onto the DODA–clay layer. Step 3: Grafting of C_{60} onto the DODA–clay–DODA monolayer. This cycle (steps 1–3) could be repeated as many times as required. Right column: The sample morphology after each step of the cycle and photographs of the substrate after steps 1 (2nd panel from the top) and 3 (4th panel from the top). Bottom left: The final product.

Results and Discussion

The sequential-deposition procedure that enabled the molecularly controlled synthesis of the hybrid films is shown in Figure 1 (for a color version, see the Supporting Information). The deposition procedure was composed of three main steps: In the first step, a DODA–clay monolayer was prepared at the air/water interface and transferred onto the substrate. Unlike with conventional Langmuir–Blodgett or Langmuir–Schaefer deposition techniques, the subphase was a mixture of ultrapure water and clay (very low clay loading: 10 ppm; Figure 1, top right). In the second step, the DODA–clay layer was dipped into a solution of DODA to allow for the self-assembly of DODA on the remaining unfunctionalized side of the clay (Figure 1, central panel). Third, the DODA–clay–DODA-covered substrate was lowered into a solution of C_{60} for self-assembly (Figure 1, bottom right). The whole nanofabrication cycle (steps 1–3) could be repeated as many times as required to achieve the desired number of C_{60} layers. For more details about the exact conditions and concentrations, see the Experimental Section.

The successful transfer of the hybrid layers was deduced from the plots of the surface pressure (measured from the Langmuir–Blodgett trough) and total film area versus time (Figure 2). The stepped line represents the total trough area that was covered by the hybrid monolayer that could be transferred onto a substrate at each time interval. At the be-

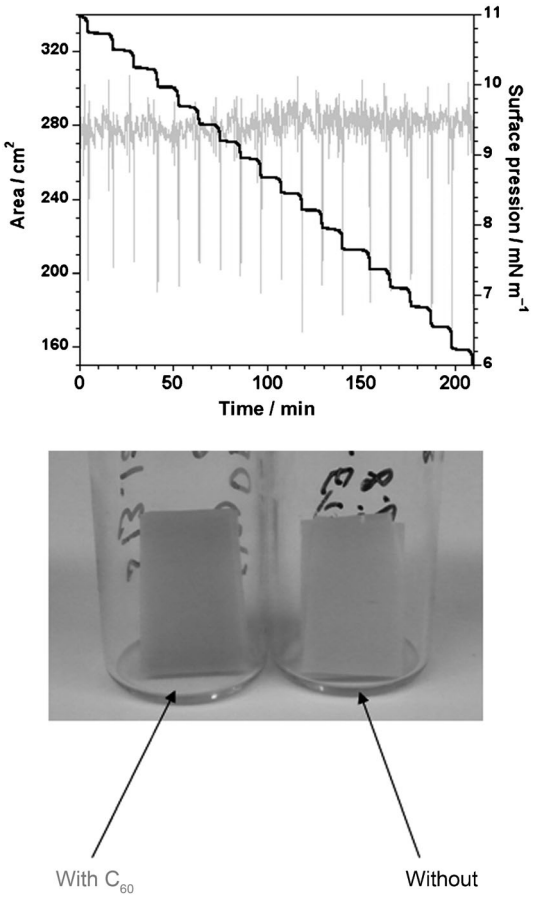

Figure 2. Upper panel: The black curve corresponds to the trough area that was covered by a hybrid DODA–clay monolayer, which could be transferred onto a substrate, during the deposition of a 19-layer DODA–clay–DODA–C_{60} film. The gray curve shows the stable surface pressure (about 9.5 mN m^{-1}). Lower panel: Photographs of 40-layer DODA–clay–DODA–C_{60} and DODA–clay–DODA films that were deposited onto mylar.

ginning of an experiment, the trough barriers were extended and the air/water interface was fully covered by a stable monolayer. As a function of time, when the substrate was dipped into the subphase, the total trough area decreased owing to the transfer of a single layer from the air/water interface onto the substrate during each dip step. This transfer was visible as a sharp step in the curve. If the step height (which gave an area value) was equal to the substrate surface area, then the transfer ratio was 1 and the surface was 100% covered by the hybrid layer each time it was lowered into the subphase. A transfer ratio that was different from unity indicated excess (multilayer) transfer or a lack of transfer (incomplete coverage). The curve shown in Figure 2 is a typical example of such a curve that was recorded during the deposition of a 19-layer-thick hybrid DODA–clay–DODA–C_{60} film. The transfer ratio was close to 1 throughout the deposition, thereby testifying to a successful transfer during each dip step. Moreover, a change in hydrophobicity was observed (Figure 1, right panel), which attested to the change in surface termination during one cycle; from hydrophilic (clay-terminated, step 1) to hydrophobic (DODA-terminated, steps 2,3).

To gain an insight into the integration of C_{60} guest molecules between the clay platelets, we compared DODA–clay–DODA and DODA–clay–DODA–C_{60} films by using temperature-dependent XRD measurements. With this technique, we determined the d_{001} basal spacing of the hybrid clay structure. Figure 3 shows the XRD patterns of 80-layer-

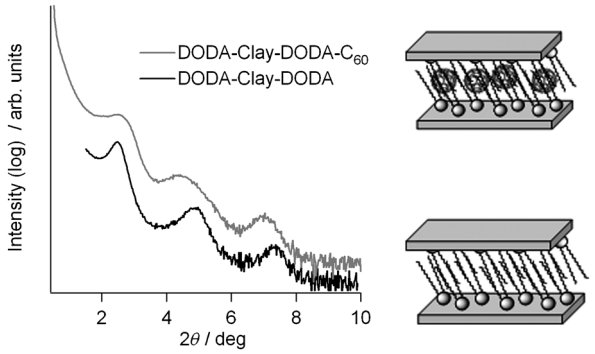

Figure 3. Temperature-dependent XRD patterns of 80-layer-thick DODA–clay–DODA and DODA–clay–DODA–C_{60} films that were deposited onto glass and sketches of their corresponding expected structures.

thick films of DODA–clay–DODA and DODA–clay–DODA–C_{60} that was deposited onto glass. A first glance revealed some differences between the patterns. The C_{60}-containing sample showed peaks that were slightly broader and shifted towards lower angles compared to the pure organoclay DODA–clay–DODA sample. These observations revealed a slight increase in the d-spacing for the C_{60}-containing sample and an increased disorder owing to the presence of C_{60} in the interlayer space. Because the surfactant layers were deposited in steps 1 and 2 (Figure 1) under exactly the same conditions (concentration and time), for both samples, the density of the deposited surfactant was expected to be identical. (For a discussion regarding the angle between the surfactant and the clay surface, see a previous study of the DODA–clay–DODA structure.[28]) Therefore, we deduced that C_{60} was accommodated between the double alkyl chains of the surfactant and not on top of it, and hence it did not significantly affect the organoclay structure. To confirm the presence of C_{60} in the hybrid structure, we annealed both samples to eliminate the surfactant molecules. The DODA–clay–DODA and DODA–clay–DODA–C_{60} diffraction patterns (Figure 4a and b, respectively) were recorded during a step by step annealing at the indicated temperatures, starting from room temperature up to 320°C. By using the Bragg formula, from these data, we extracted the d-spacing (Figure 5) as a function of the annealing temperature. Starting from above 180°C, which was the melting point of DODA, for both the DODA–clay–DODA and the DODA–clay–DODA–C_{60} films, the d-spacing was reducing as a function of temperature. However, the most-interesting feature

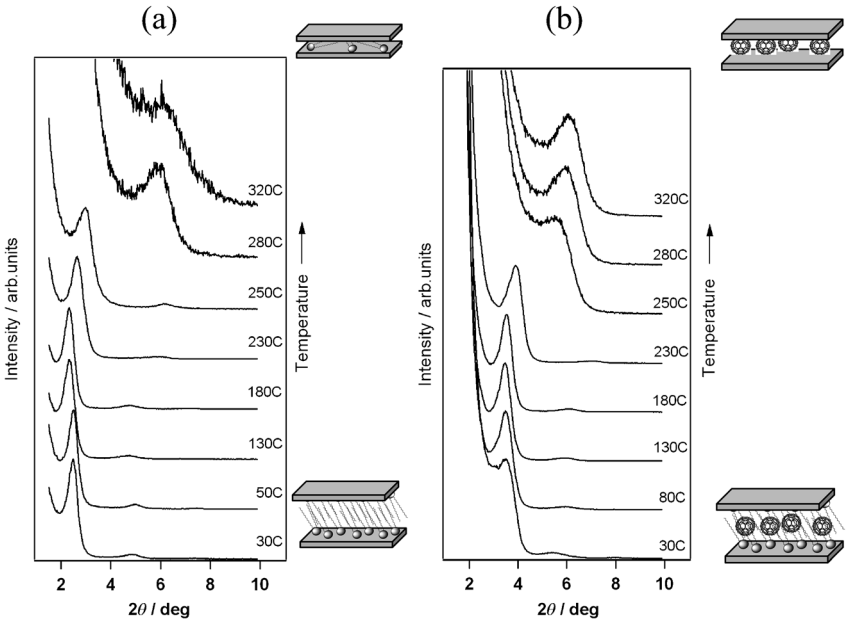

Figure 4. Temperature-dependent XRD patterns of 80-layer-thick DODA–clay–DODA (a) and DODA-clay-DODA-C_{60} films (b) that were deposited onto glass and sketches of their corresponding expected structures.

Scherrer equation. We observed values of 200(±10) Å for the as-deposited film and 73-(±17) Å after annealing. Once converted into layer units, these coherence lengths corresponded to about 7 layers for the starting material and about 5(±1) layers for the annealed material. Therefore, we concluded that a slight increase in disorder was induced by the melting and de-intercalation of the DODA molecules.

XPS not only gives the elemental composition of a surface, it is also sensitive to the chemical environment of each element. The bottom left panel in Figure 6 shows a comparison of the C 1s photoemission lines of the as-deposited DODA–clay–

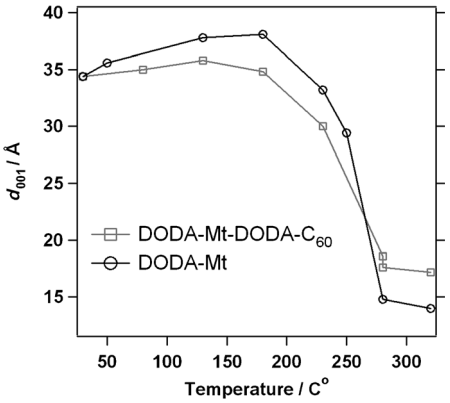

Figure 5. Values of d(001) that were extracted from the XRD patterns of DODA–clay–DODA and DODA–clay–DODA–C_{60} films that were recorded at different temperatures. The final d_{001} spacings were 16.2 and 13.8 Å for samples with and without C_{60}, respectively.

was the difference in the final d-spacing of the two samples: about 13.8 (±0.3) and 16.2 (±0.2) Å for the layers without and with fullerene, respectively. This observation confirmed the successful insertion of C_{60} molecules between the clay sheets; in fact, it was the presence of C_{60} (bulk C_{60} decomposed at 900 K[33,34]) that kept the clay from collapsing to a lower d-spacing by creating a stable pillared clay structure. One could argue that the value of the final d-spacing of the pure organoclay was about 1–2 Å too thick; we assigned this mismatch to the inevitable presence of cations inside the clay stack (see the discussion of X-ray photoelectron spectroscopy data below), which was necessary to achieve charge neutrality. The size of the coherently diffracting domains could be estimated from the peak width by using the

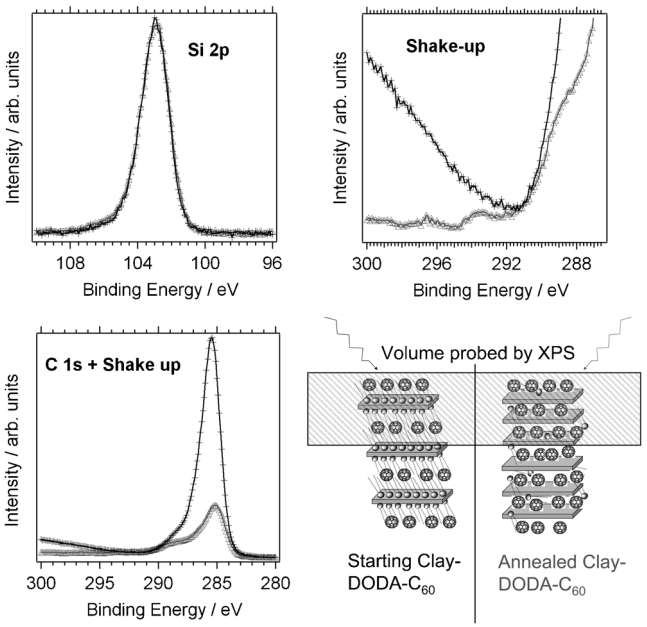

Figure 6. XPS of the normalized C 1s and Si 2p core-level regions for a 50-layer-thick DODA–clay–DODA–C_{60} film that was deposited onto glass before (black lines) and after annealing at 350 °C (gray lines); Top left: Enlargement of the C 1s shake-up region; Bottom right: Structure of the samples.

DODA–C_{60} film with the same lines after stepwise annealing at up to 320 °C. There was a dramatic difference in intensity between the as-deposited film and the annealed one (both were normalized to the Si 2p photoemission intensity). The three-times-higher carbon content of the as-deposited film surface could be explained by the film structure

(Figure 6, bottom): before annealing, the film was expected to be composed of C_{60} molecules that were intercalated among the long aliphatic chains of DODA and sandwiched between the clay platelets (see above), whilst after annealing, only clay and C_{60} should have been present. Because the probing depth of XPS was limited to the first few nm, carbon from the long aliphatic chains of DODA dominated the spectrum before annealing, whilst after annealing, when most of the DODA has de-intercalated, the structure had shrunk and C_{60} prevailed in the C 1s spectrum (Figure 3). For the same reason, the observed Si/C ratio also varied. The high-binding-energy region next to the C 1s peak (Figure 6, top right) confirmed this conclusion: before annealing, the typical C_{60} shake-up structure[35] was not visible because it was attenuated by DODA; however, after heat treatment, it was clearly distinguishable, thereby confirming the presence of C_{60} within the clay stack.

Although great care was taken in sample handling to minimize contamination, we could not totally exclude the presence of adventitious carbon because the sample was prepared under atmospheric conditions. Nevertheless, whilst adventitious carbon might affect the line-shape of the main C 1s photoemission line, the observed shake-up structure was an unmistakable signature of C_{60}.

The N 1s core line clearly confirmed the presence of surfactant molecules. In both the survey spectrum and the detailed scan (see the Supporting Information), the N 1s peak for the as-deposited film was observed but not for the annealed film, which also supported the structural model before and after heat treatment (see above). The observed nitrogen signal arose from the cyanide bond ($CN^*{-}CN^{*+}$) of the ammonium head-group of the surfactant. The corresponding carbon–nitrogen bond ($C^*N{-}C^*N^+$) was probably responsible for the shoulder that appeared on the high-binding-energy side of the C 1s lines (Figure 6) at binding energies of about 286–288 eV. Occasionally, we also found spectroscopic evidence for a minute amount of sodium, which was presumably owing to an incomplete cation-exchange reaction on the clay during deposition steps 1 and 2 (Figure 1), where Na^+ ions were replaced by DODA. Optical photographs of the samples also supported the successful insertion of C_{60} between the clay sheets (Figure 2, right; for a color version, see the Supporting Information): the 40-layer DODA–clay–DODA–C_{60} film was darker than the 40-layer DODA–clay–DODA film; both were deposited onto mylar. This darker color was due to light absorption by C_{60}.[36]

Microscopy is an extremely useful tool for the characterization of layers in terms of roughness and homogeneity. STM images of single layers of DODA–clay–DODA–C_{60} that were deposited onto Au are shown in Figure 7 and Figure 8. Even at high magnification, the film was uniform and C_{60} molecules evenly covered the surface. The C_{60} molecules were ball-shaped objects with an estimated diameter of 6–7 Å (Figure 7 and Figure 8). Scanning the same area for a few minutes induced dynamic processes, as observed by comparing the images in Figure 8. Some C_{60} molecules remained immobile whilst others moved or even disappeared from the scanned area. (video available online at http://www. chemeurj.org). This result confirmed the detachment of some C_{60} molecules from DODA owing to molecule–tip interactions. We also observed that the C_{60} molecules stopped moving when they aggregated into chains (Figure 8, black rectangles), presumably owing to stronger bonding with neighboring C_{60} molecules than with the surfactant. Interestingly, we observed that the aggregation of C_{60} was quite low compared to what one would expect[38,39] on unfunctionalized surfaces, such as graphite. To the best of our knowledge, STM of C_{60} molecules on organic templates (the surfactant self-assembled layer) is still rather unexplored (Li et al.[37] reported an STM study of C_{60} within, but not on, a self-assembled monolayer).

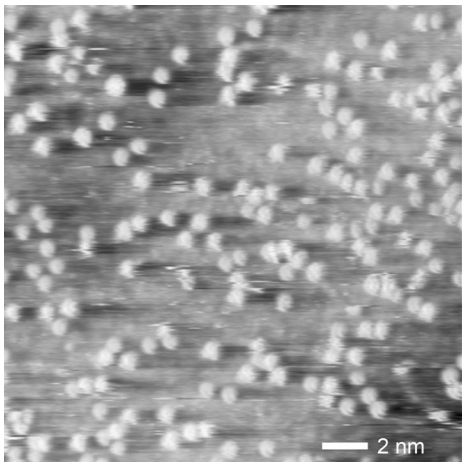

Figure 7. STM images of a single layer of DODA–clay–DODA–C_{60} that was deposited onto a gold substrate; images were recorded at 300 K, tunneling conditions: 1.1 V at 150 pA

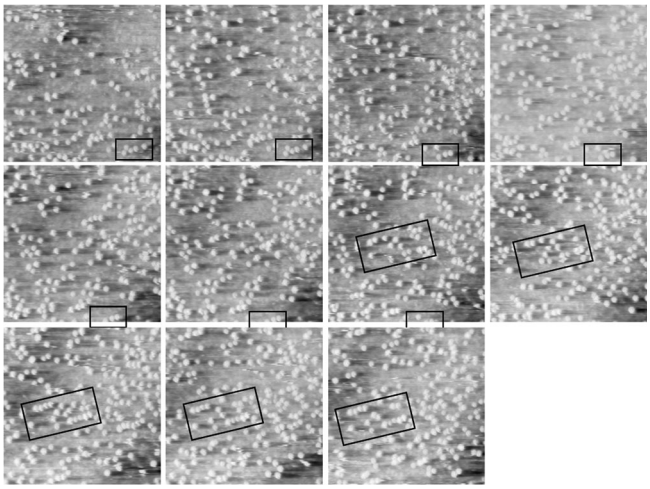

Figure 8. A sequence of ambient STM images of a single layer of DODA–clay–DODA–C_{60} that was deposited onto a gold substrate; images were recorded at 300 K, tunneling conditions: 1.1 V at 150 pA. Image dimensions: 20nm × 20nm.

Conclusion

The controlled layer-by-layer deposition of hybrid films in which C_{60} molecules are inserted between aluminosilicate layers and surrounded by surfactant molecules has been performed. The deposition was performed by using an organic–inorganic hybrid Langmuir–Schaefer approach. Characterization of the hybrid films by X-ray diffraction showed clear evidence of a layered structure and the existence of a pillared layer structure after annealing. X-ray photoelectron spectroscopy allowed us to observe the C_{60} signature, and STM showed that the bi-dimensional array of C_{60} was rather dense.

The effectiveness of this method in terms of coverage and uniformity was clearly superior to previously reported results (the bulk intercalation of water-soluble fulleropyrolidine derivatives[18,19]). In this earlier procedure, the simple mixing of the various components without control of the sequencing of the assembly showed non-uniform intercalation and only rarely showed the presence of C_{60} in the stack. Conversely, the method presented herein is much more robust, thereby yielding high coverage and single-layer-level control of the assembly. This fabrication route opens new perspectives for the design and construction of functional organic–clay hybrid materials.

Experimental Section

Materials: The clay used for the preparation of the hybrid films was a natural sodium-saturated montmorillonite Kunipia F clay that was provided by Kunimine Industries Co. (Japan) with the structural formula $Ca_{0.11}Na_{0.891}(Si_{7.63}Al_{0.37})(Al_{3.053}Mg_{0.65}Fe_{0.245}Ti_{0.015})\cdot O_{20}(OH)_4$ and a cation-exchange capacity (CEC) of 1.18 meq g^{-1} of clay. The stock dispersion of the clay (1 g) was prepared by stirring the clay for 12 h in Millipore ultrapure water (1 L). The dispersion was diluted to a given concentration with pure water before being used as a subphase in the Langmuir–Schaefer deposition.

Dimethyldioctadecylammonium (DODA) bromide (purity >99%, Sigma–Aldrich) was used as received (structural formula $[\{CH_3(CH_2)_{17}\}_2N(Br)(CH_3)_2]$). DODA was dissolved (0.1 mg mL^{-1}) in a mixture of HPLC-grade $CHCl_3$ and MeOH (9:1, v/v) to prepare the spreading solution. For surface modification, a mixture of EtOH and pure water (8:2, v/v) of DODA (0.5 mg mL^{-1}) was used.

Preparation of the hybrid films: All of the films were prepared according to the deposition cycle shown in Figure 1 by means of a Nima Technology thermostated 612D Langmuir–Blodgett (LB) trough at a temperature of 21(±0.5) °C. The pressure sensor used a Wilhemly plate (small length of chromatography paper) to measure the surface pressure (reduction in surface tension). Pure water and clay dispersions in Millipore Q-grade water were used as a subphase. A clay concentration of 10 ppm in the dispersion was chosen as the optimal value.[28] Depending on the requirements of the characterization method, samples were either deposited on a 150 nm gold film on mica for STM or on SiO_2 or glass substrates for XRD and XPS. First, a solution of DODA (0.1 mg mL^{-1}) in $CHCl_3$/C_2H_5OH (9:1, 200–300 mL) was injected at the air/water interface. After 20–30 min to allow hybridization to occur, the hybrid DODA–clay layer at the air/water interface was compressed at a rate of 30 cm^2 min^{-1} until the chosen stabilization pressure of 13 mN m^{-1} was reached. This pressure was maintained throughout the deposition process. Films were deposited by horizontal lift onto one of the above-mentioned substrates, with downward and lifting speeds of 10 and 2 mm min^{-1}, respectively. Samples were allowed to touch the water (very gentle dip, of max 0.5 mm below the water level) and rinsed directly after dipping in 18 mΩ MilliQ water to eliminate any weakly attached cations that remained from the hybridization process.

To graft C_{60} onto the clay surfaces, a linker was needed; in this experiment, the linker was a self-assembled monolayer of DODA. As shown in Figure 1, the freshly deposited DODA–clay monolayer was lowered into a mixture of DODA (1 mg mL^{-1}) in ethanol/water (9:1) to form a DODA–clay–DODA layer. Again, the sample was cleaned with 18 MΩ MilliQ water to remove any excess material from the sample surface. During the first hybridization step, when clay and DODA reacted through the cation exchange/attachment of the DODA molecules at the clay sheet surface within the LB trough and during the previously mentioned, chemically identical second hybridization, sodium was substituted by DODA. The XPS data confirmed this cation-exchange process. The final step of this deposition procedure was a 2 min lowering of the hybrid layer (DODA–clay–DODA) into a solution of C_{60} (0.2 mg mL^{-1}; sublimed, 99.9%, Sigma Aldrich, used as received) in toluene (sigma Aldrich, 99.5%, used as received), which was prepared by the mixing and short sonication (~1 min). This step was followed by rinsing with 18 mΩ MilliQ water. To avoid contaminating any of the other solutions or, more importantly, the LB air-water interface, with water, all samples were dried under a flow of nitrogen after each washing step (steps 1–3). We observed that omitting drying a water droplet that remained on the substrate caused a disruption of the LB stabilization. To go from a single layer to multilayers, one simply repeated the cycle as many times as was needed. We produced samples of 1 layer for STM and of 50–100 layers for XPS and XRD analysis.

X-ray diffraction (XRD): XRD patterns were collected by using a Philips PANanlytical X′Pert MRD diffractometer with a $Cu_{K\alpha}$ ($\lambda = 1.5418$ Å) radiation source (40 kV, 40 mA), a 0.25° divergent slit and a 0.125° antiscattering slit. The diffracted intensity was recorded in the range $2\theta = 0.5$–10° with a 0.02° step and counting time of 10 s per step for the non-ambient measurements in a temperature range of 25–320°.

X-ray photoelectron spectroscopy (XPS): Photoemission spectra were collected on a SSX-100 (Surface Science Instruments) spectrometer that was equipped with a monochromatic Al Kα X-ray source (1486.6 eV) and operating in a base pressure of 5×10^{-10} mbar. The energy resolution was set to 1.3 eV and the photoelectron take-off angle was 37°. A flood gun that provided electrons with 0.1 eV kinetic energy, in combination with a Mo grid that was placed above the sample, was used to compensate for sample charging. All binding energies were referenced to the Si 2p peak of clay at 102.9 eV.[30,31] Spectroscopic analysis included a Shirley background subtraction.[32]

Scanning tunneling microscopy (STM): STM images of the hybrid DODA–clay–DODA and DODA–clay–DDA–C_{60} layers were recorded in the constant current mode at RT in air by using a Molecular Imaging STM with Pt/Ir mechanically cut tips. Data treatment included plane subtraction, smoothing, and adjustment of the color scale and brightness to enhance the contrast.

Acknowledgements

L.M.T. acknowledges E.U. support through the EIF-041956 Marie Curie fellowship. Financial support from the Dutch Foundation for Fundamental Research on Matter (FOM), the Breedtestrategie program of the University of Groningen, and the MSC+ program of the Zernike Institute for Advanced Materials is gratefully acknowledged.

[1] D. M. Guldi, F. Zerbetto, V. Georgakilas, M. Prato, *Accounts Chem. Res.* **2005**, *38*, 38–43.

[2] N. A. Kotov, F. C. Meldrum, J. H. Fendler, E. Tombacz, I. Dekany, *Langmuir* **1994**, *10*, 3797–3804.

[3] B. Bröker, O. T. Hofmann, G. M. Rangger, P. Frank, R. P. Blum, R. Rieger, L. Venema, A. Vollmer, K. Müllen, J. P. Rabe, A. Winkler, P. Rudolf, E. Zojer, N. Koch, *Phys. Rev. Lett.* **2010**, *104*, 246805.
[4] T. J. Pinnavaia, *Science* **1983**, *220*, 365–371.
[5] J. Konta, *Appl. Clay Sci.* **1995**, *10*, 275–335.
[6] J. A. Ballantine, *NATO ASI Ser., Ser. C* **1986**, *165*, 197.
[7] V. Georgakilas, D. Gournis, D. Petridis, *Angew. Chem.* **2001**, *113*, 4416–4418; *Angew. Chem. Int. Ed.* **2001**, *40*, 4286–4288.
[8] V. Georgakilas, D. Gournis, A. B. Bourlinos, M. A. Karakassides, D. Petridis, *Chem. Eur. J.* **2003**, *9*, 3904–3908.
[9] B. K. G. Theng, *The Chemistry of Clay Organic Reactions*, Adam Hilger, London, **1974**.
[10] A. Gil, L. M. Gandia, M. A. Vicente, *Catal. Rev.* **2000**, *42*, 145–212.
[11] K. Inukai, Y. Hotta, S. Tomura, M. Takahashi, A. Yamagishi, *Langmuir* **2000**, *16*, 7679–7684.
[12] T. Shichi, K. J. Takagi, *Photochem. Photobiol., C* **2000**, *1*, 113–130.
[13] A. F. Hebard, M. J. Rosseinsky, R. C. Haddon, D. W. Murphy, S. H. Glarum, T. T. M. Palstra, A. P. Ramirez, A. R. Kortan, *Nature* **1991**, *350*, 600–601.
[14] P. M. Allemand, K. C. Khemani, A. Koch, F. Wudl, K. Holczer, S. Donovan, G. Gruner, J. D. Thompson, *Science* **1991**, *253*, 301–303.
[15] L. W. Tutt, A. Kost, *Nature* **1992**, *356*, 225–226.
[16] V. Georgakilas, F. Pellarini, M. Prato, D. M. Guldi, M. Melle-Franco, F. Zerbetto, *P. Natl. Acad. Sci. USA* **2002**, *99*, 5075–5080.
[17] N. Tagmatarchis, M. Prato, *Pure Appl. Chem.* **2005**, *77*, 1675–1684.
[18] D. Gournis, V. Georgakilas, M. A. Karakassides, T. Bakas, K. Kordatos, M. Prato, M. Fanti, F. Zerbetto, *J. Am. Chem. Soc.* **2004**, *126*, 8561–8568.
[19] D. Gournis, L. Jankovic, E. Maccallini, D. Benne, P. Rudolf, J. F. Colomer, C. Sooambar, V. Georgakilas, M. Prato, M. Fanti, F. Zerbetto, G. H. Sarova, D. M. Guldi, *J. Am. Chem. Soc.* **2006**, *128*, 6154–6163.
[20] Y. Hotta, M. Taniguchi, K. Inukai, A. Yamagishi, *Langmuir* **1996**, *12*, 5195–5201.
[21] M. Ogawa, A. Ishikawa, *J. Mater. Chem.* **1998**, *8*, 463–467.
[22] K. Tamura, H. Setsuda, M. Taniguchi, A. Yamagishi, *Langmuir* **1999**, *15*, 6915–6920.
[23] Y. Ogata, J. Kawamata, C.-H. Chong, M. Makihara, A. Yamagishi, G. Saito, *Mol. Cryst. Liq. Cryst. Sci. Technol. Sect. A* **2002**, *376*, 245–250.
[24] Y. Umemura, *J. Phys. Chem. B* **2002**, *106*, 11168–11171.
[25] Y. Umemura, Y. Einaga, A. Yamagishi, *Mater. Lett.* **2004**, *58*, 2472–2475.
[26] T. Yamamoto, Y. Umemura, O. Sato, Y. Einaga, *Chem. Mater.* **2004**, *16*, 1195–1201.
[27] T. Yamamoto, Y. Umemura, O. Sato, Y. Einaga, *Chem. Lett.* **2004**, *33*, 500–501.
[28] L. M. Toma, R. Y. N. Gengler, E. B. Prinsen, D. Gournis, P. Rudolf *Phys. Chem. Chem. Phys.* **2010**, *12*, 12188–12197.
[29] L. M. Toma, R. Y. N. Gengler, D. Cangussu, E. Pardo, F. Lloret, P. Rudolf, *J. Phys. Chem. Lett.* **2011**, *2*, 2004–2008.
[30] T. L. Barr, *Appl. Surf. Sci.* **1983**, *15*, 1–35.
[31] J. K. Moulder, P. E. Sobol, K. D. Bomben, *Handbook of X-ray photoelectron Spectroscopy*; Eden Prairie: Minnesota, **1995**.
[32] D. A. Shirley, *Phys. Rev. B* **1972**, *5*, 4709–4709.
[33] C. S. Sundar, A. Bharathi, Y. Hariharan, J. Janaki, V. Sankara Sastry, T. S. Radhakrishnan, *Solid State Commun.* **1992**, *84*, 823–826.
[34] S. D. Leifer, D. G. Goodwin, M. S. Anderson, J. R. Anderson, *Phys. Rev. B* **1995**, *51*, 9973–9973.
[35] A. J. Maxwell, P. A. Bruhwiler, A. Nilsson, N. Martensson, P. Rudolf, *Phys. Rev., B* **1994**, *49*, 10717–10717.
[36] J. Shinar, Z. V. Vardeny, Z. H. Kafafi, *Optical and Electronic Properties of Fullerenes and Fullerene-Based Materials*, CRC Press, **2000**.
[37] F. Li, L. Tang, W. Zhou, Q. Guo, *J. Phys. Chem. C* **2009**, *113*, 17899–17903.
[38] H. Yu, Y. Li, W. S. Yang, Z. Gu, Y. Wu, *Surf. Sci.* **1993**, *286*, 116–121.
[39] P. R. Hui Liu, *J. Chem. Phys.* **2006**, *124*, 164707.

Received: November 9, 2011
Revised: February 10, 2012
Published online: April 20, 2012

